



## Staff Summary Sheet

	To	Action	Signature (Surname), Grade, Date		To	Action	Signature (Surname), Grade, Date
1	DFEM	Approve	 5-6, 11 APR 13	6			
2	DFER	Review	 16 APR 13	7			
3	DFEM	Action		8			
4				9			
5				10			

Grade and Surname of Action Officer Dr. Lubov P. Andrusiv	Symbol DFEM	Phone 333-9095	Suspense Date 28 April 2013
Subject Clearance of Material for Public Release      Case Number: <b>USAFA-DF-PA-287</b>			SSS Date 11 April 2013

### Summary

**1. Purpose:** To provide security and policy review on the document at Tab 1 prior to release to the public.

### 2. Background:

- *Author(s):* Dr. Lubov P. Andrusiv, USAFA, DFEM/DFRL

~~Dr. Christopher M. Richards, University of Louisville, ME Department~~

- *Title:* Configuration Control of Telescoping Beams with Three or More Segments

- *Abstract:* This paper the possibility of controlling the dynamic response of telescoping structures with three or more segments by adjusting the position of the middle segment or segments independently of the total length of the beam.

- *Release information:* To be submitted to the Journal of Sound and Vibration or International Journal of Solids and Structures.

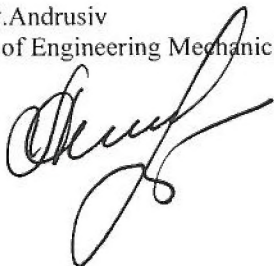
- *Previous clearance information:* 1. Article (DF-PA-366) for publishing in Journal of Fracture Mechanics, 2010. 2. The conference paper (DF-PA-367) for presenting on the VIII Int'l Conference in Ukraine, 2010. 3. Article (DF-PA-527) for ASME Journal of Vibration and Acoustics, 2011.

- *Recommended distribution statement:* Distribution A, Approved for public release, distribution unlimited.

### 3. Discussion:

### 4. Recommendation:

Dr. Lubov P. Andrusiv  
Department of Engineering Mechanics



Tab  
1. Copy of article

# **CONFIGURATION CONTROL OF TELESCOPING BEAMS WITH THREE OR MORE SEGMENTS**

**Lubov P. Andrusiv**

United States Air Force Academy, Department of Engineering Mechanics,  
Colorado Springs, CO 80840-6252

## **ABSTRACT**

This research addresses the possibility of controlling the dynamic response of telescoping beams with three or more segments by adjusting the position of the middle segment or segments independently of the total beam length. As part of this work, the idea of a beam “configuration space” is introduced, and the dependence of the response on the nature of the deployment and retraction processes is discussed. Concepts for presentation of solution results in the form of nondimensional design charts are also presented.

## **1. Problem Background**

The subject of this research is segmented, telescoping, beam-like structures. Such structures represent an important class of engineering systems with nonuniform geometric and physical parameters. They are characterized by multiple segments that can retract inside of, or relative to one another during operation. Examples include variable focal-length telescopes, pneumatic and hydraulic cylinders, cranes and ladders, extensible booms, antennas, robotic arms, and deployable space structures.

Most telescoping systems are quite compliant and prone to vibration problems, yet require accurate positioning in order to function properly. Their inertia and compliance distributions change during operation, and the new distributions affect dynamic response. These changes make it difficult to tune parameters in a manner that avoids all potential problems.

Because vibration problems are so likely in multi-segmented telescoping beam structures, they should be subjected to modal analysis. Such analyses require an appropriate mathematical model which must reflect the complex interactions that occur among the segments during deployment and retraction. These interactions in turn produce a very complicated spatial and temporal redistribution of stiffness and inertia properties whose effect on performance and stability needs to be understood.

Dynamic modeling and detailed understanding of the vibrational modes of such systems are necessary to know how the system will respond to excitation by external forces and initial conditions that may be either anticipated or unanticipated and develop effective vibration suppression techniques. Some systems are particularly sensitive to vibration problems. Accordingly, vibration analysis is a fundamental part of the design process for many systems.

This work focuses on three-segment cantilevered telescoping beams with one fixed end and one free end. This focus is a result of the preponderance of this configuration in practical systems. The three-segment telescoping systems are approximated as undamped transversely vibrating structures (beams), meaning that longitudinal and torsional motions are neglected. Such an assumption is justified by the fact that many of these systems are designed to carry transverse loads, and thus transverse modes are most likely to be excited.

Mathematical modeling and solution methodologies of such telescoping mechanical systems are completely described in [1] and [2]. Specifically, such systems are modeled as transversely deflecting cantilevered beams with overlapping sections of varying length. These systems are characterized according to their physical configurations and constraints. The equation of motion for these systems is based on classical continuous beam theory upon multiple applications of the Euler-Bernoulli partial differential equation to the beam domain. The frequency equation (an amalgamation of trigonometric and hyperbolic terms, in this case) is



expressed in the form of a determinant equated to zero. An efficient algorithm for solving eigenproblem embodied in this determinant equation is presented and discussed in details. An initial example case study illustrates application of the free and forced vibration problem formulation methodologies, implementation of the solution methodologies, and interpretation of the results.

To study the kinematics of the deployment process of the telescoping structures, which is the objective of this paper, the principal model of three segment telescoping system and its sectioning model presented in [1] needs to be recalled here. The principal model is shown in Figure 1.1.

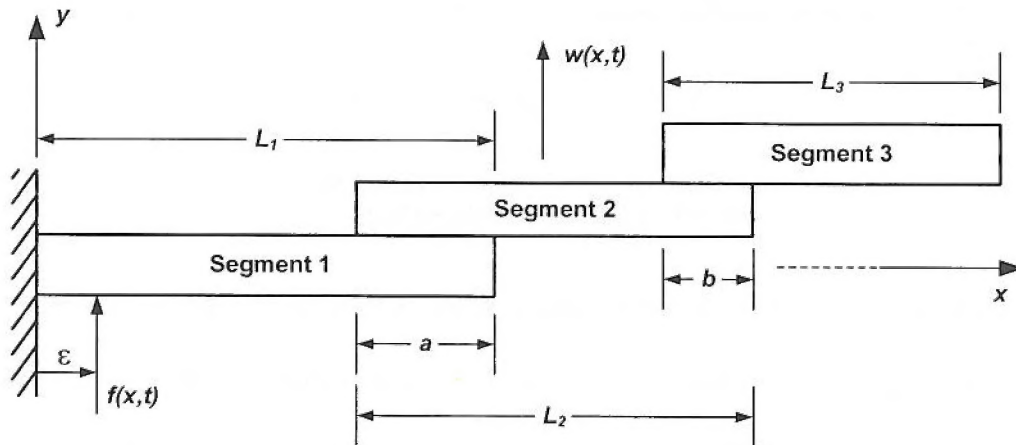
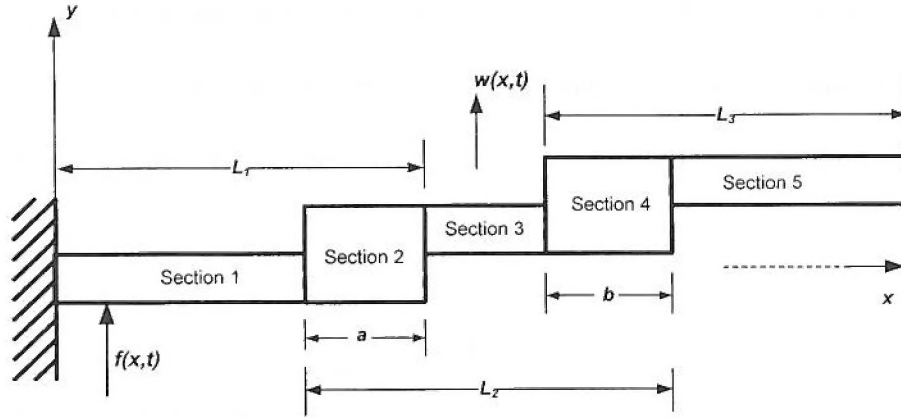


Figure 1.1. Three-segment cantilever beam with overlapping sections  $a$  and  $b$ .

In this figure the term “segment” refers to a physically contiguous portion of the beam structure than cannot telescope upon itself. A segment typically consists of a single component of fixed length. In this research, opening processes are referred to as “deployment,” or less frequently, “extension.” Closing processes are referred to as “retraction.” If two segments overlap during operation of the telescoping beam ( $a$  and  $b$  in Figure 1.1), the longitudinally coincident portion of the two segments will form a new section, with section properties determined by the behavior of the composite cross section. Sections of this type are referred to

as “overlap sections.” Upon application of the distributed-parameter Euler-Bernoulli sectioning method, the beam is modeled as shown in Figure 1.2, with five sections, of which two, section 2 and section 4, are overlap sections. For known segment lengths, specification of the overlap section lengths completely fixes the longitudinal configuration of a telescoping beam, regardless of the boundary conditions, overlap section constraints, or number of segments.<sup>1</sup>



**Figure 1.2 Division of a three-segment telescoping beam into distributed parameter Euler-Bernoulli sections.**

To complete the parameterization of the model requires specification of the segment lengths,  $L_1$ ,  $L_2$ , and  $L_3$ , the section flexural rigidities,  $EI(x)$ , and section densities,  $\rho$ . Also in Figures 1 and 2,  $w(x, t)$  represents the transverse displacement of the beam from its equilibrium position, and  $f(x, t)$  is any external transverse force that might be acting upon the beam. Also, it needs to be mentioned that in this model the connection between the segments of the beam is tight so that a cross section at the overlap can be considered as continuous and behaves as a single solid section. Euler-Bernoulli fourth order partial differential equation of motion is formulated in [1] for each beam section, and expressed for the complete five-section beam by equation (1) recalled below

<sup>1</sup> This conclusion, while important, is not as profound as it might appear. Some beam configurations will have overlap sections comprised of more than two segments. In nearly retracted configurations, the number of overlap segments will exceed the number of single segment sections.

$$E^{[i]} I^{[i]} \frac{\partial^4 w^{[i]}(x, t)}{\partial x^4} + \rho^{[i]} A^{[i]} \frac{\partial^2 w^{[i]}(x, t)}{\partial t^2} = f^{[i]}(x, t) \quad (1)$$

## 2. Nondimensionalizing the Telescoping Beam Equation of Motion

### 2.1 Free Undamped Vibration Solution

In the absence of any excitations, when  $f(x, t) = 0$ , the homogeneous part of the differential equation of vibrating motion (1) provides the basis for the study the modal characteristics of the segmented beam at various stages of the deployment. Consequently, the eigenvalues and corresponding eigenfunctions can be obtain by the eigensolution to the equation

$$E^{[i]} I^{[i]} \frac{\partial^4 w^{[i]}(x, t)}{\partial x^4} + \rho^{[i]} A^{[i]} \frac{\partial^2 w^{[i]}(x, t)}{\partial t^2} = 0 \quad (2)$$

Here the superscript  $[i]$  indicates that the associated parameter applies only to the  $i$ -th beam section. For a modal analysis or a free vibration solution, it is convenient to separate variables as follows:

$$w^{[i]}(x, t) = W^{[i]}(x)T(t) = W^{[i]}(x)e^{\omega t} \quad (3)$$

Substituting equation (3) into equation (2), the partial differential equation of motion can be separated into two ordinary differential equations in a form

$$\frac{d^4 W^{[i]}(x)}{dx^4} + \left( \frac{\omega^2 \rho^{[i]} A^{[i]}}{E^{[i]} I^{[i]}} \right) W^{[i]}(x) = 0 \quad (4)$$

where  $\omega^2$  is the separation constant and should be positive due to the nature of the vibration problem. The physical interpretation of  $\omega$  is a natural frequency of the system. The spatial variables  $W$  (transverse displacement) and  $x$  (beam axial position) in equation (4) can be normalized by dividing by a reference length  $L_r$ :

$$\bar{W}^{[i]} = \frac{W^{[i]}}{L_r}; \quad \bar{x} = \frac{x}{L_r}; \quad (5)$$

While a different reference length could be used for each section, it is convenient to normalize individual section length with a common  $L_r$  value. This approach makes it easier to reproduce the mode shapes or displacement patterns after the solution is complete. A good choice of  $L_r$  for a telescoping beam, where the net length tends to change, is the length of segment 1, which remains constant. A non-physical length ( $L_r = 1.0$ , for example, is also a reasonable choice).

The first spatial derivative and higher derivatives of the first term in equation (3) now become:

$$\frac{dW^{[i]}(x)}{dx} = \frac{dL_r \bar{W}^{[i]}(x)}{dx} = \frac{L_r d\bar{W}^{[i]}(\bar{x})}{d\bar{x}} \frac{d\bar{x}}{dx} = \frac{L_r d\bar{W}^{[i]}(\bar{x})}{d\bar{x}} \left( \frac{1}{L_r} \right) = \frac{d\bar{W}^{[i]}(\bar{x})}{d\bar{x}} \quad (6)$$

$$\frac{d^n W^{[i]}(x)}{dx^n} = \left( \frac{1}{L_r} \right)^{n-1} \frac{d^n \bar{W}^{[i]}(\bar{x})}{d\bar{x}^n} \quad (7)$$

respectively, and the equation of free motion itself reduces to:

$$\left( \frac{1}{L_r^3} \right) \frac{d^4 \bar{W}^{[i]}(\bar{x})}{d\bar{x}^4} + \left( \frac{\omega^2 \rho^{[i]} A^{[i]}}{E^{[i]} I^{[i]}} \right) L_r \bar{W}^{[i]}(\bar{x}) = 0 \quad (8)$$

$$\frac{d^4 \bar{W}^{[i]}(\bar{x})}{d\bar{x}^4} + \omega^2 \left( \frac{\rho^{[i]} A^{[i]} L_r^4}{E^{[i]} I^{[i]}} \right) \bar{W}^{[i]}(\bar{x}) = 0 \quad (9-8)$$

To further parameterize the equation, define a dimensionless density,  $\rho_r$ , cross sectional area,  $A_r$ , modulus of elasticity,  $E_r$ , and moment of inertia,  $I_r$ . Like  $L_r$ , these reference values should be used for every section in the beam domain. The terms originally associated with the eigenvalue expressed as

$$\begin{aligned} \omega^2 \left( \frac{\rho^{[i]} A^{[i]} L_r^4}{E^{[i]} I^{[i]}} \right) &= \omega^2 \left( \frac{\bar{\rho}^{[i]} \bar{A}^{[i]}}{\bar{E}^{[i]} \bar{I}^{[i]}} \right) \left( \frac{\rho_r A_r L_r^4}{E_r I_r} \right) \\ &= \omega^2 (\alpha^{[i]})^2 \left( \frac{\rho_r A_r L_r^4}{E_r I_r} \right) \\ &= \bar{\omega}^2 (\alpha^{[i]})^2 \end{aligned} \quad (10)$$



Here  $(\alpha^{[i]})^2$  is a dimensionless physical property constant associated with a specific segment.  $\bar{\omega}$  is a dimensionless natural frequency given by

$$\bar{\omega} = \sqrt{\frac{\rho_r A_r L_r^4}{E_r I_r}} \omega \quad (11)$$

For any segment in the telescoping beam, the governing equation of motion after separation of variables becomes:

$$\frac{d^4 \bar{W}^{[i]}(\bar{x})}{d\bar{x}^4} + \bar{\omega}^2 (\alpha^{[i]})^2 \bar{W}^{[i]}(\bar{x}) = 0 \quad (12)$$

This expression is identical to equation (4) introduced earlier as an intermediate step in the eigenproblem formulation and solution. Normalization reference parameters ( $L_r$ ,  $E_r$ ,  $\rho_r$ , etc.) should be the same for each section. Provided boundary conditions are formulated in terms of the dimensionless axial position,  $\bar{x}$ , then the eigensolution will yield dimensionless natural frequencies,  $\bar{\omega}_n$ , and normalized modes,  $\bar{W}^{[i]}(\bar{x})$ . The actual natural frequencies may then be computed by inverting equation (11)

$$\omega = \sqrt{\frac{E_r I_r}{\rho_r A_r L_r^4}} \bar{\omega} \quad (13)$$

The modes will generally require amplitude normalization to meet the desired standards (a maximum transverse modal displacement of 1.0, for example). The longitudinal position scale may then be recovered by multiplying the dimensionless positions by  $L_r$ .

## 2.2 Forced Vibration Solution

Applying the same nondimensionalization process used for the unforced equation to equation (1) yields:

$$\frac{\partial^4 \bar{w}^{[i]}(\bar{x}, \bar{t})}{\partial \bar{x}^4} + \frac{\rho^{[i]} A^{[i]} L_r^4}{E^{[i]} I^{[i]} t_r^2} \frac{\partial^2 \bar{w}^{[i]}(\bar{x}, \bar{t})}{\partial \bar{t}^2} = \frac{L_r^3 f^{[i]}(\bar{x}, \bar{t})}{E^{[i]} I^{[i]}} \quad (14)$$



$$\bar{w}^{[i]} = \frac{w^{[i]}}{L_r}; \quad \bar{x} = \frac{x}{L_r}; \quad \bar{t} = \frac{t}{t_r} \quad (15)$$

Here the physical time is nondimensionalized by dividing by a reference time,  $t_r$ . One option for this value is to use the reciprocal of the fundamental frequency, which has units of  $T^{-1}$ . However this number is not a fundamental term in a particular solution to equation (14). A better choice for  $t_r$  would be 1 second.

Regardless of the value chosen for  $t_r$ , the coefficient of the acceleration term in equation (14) is dimensionless:

$$\frac{\rho^{[i]} A^{[i]} L_r^4}{E^{[i]} I^{[i]} t_r^2} \cdot \frac{\left(\frac{M}{L^3}\right)(L^2)(L^4)}{\left(\frac{F}{L^2}\right)(L^4)(T^2)} = \frac{ML/T^2}{F} \quad (16)$$

The right hand side of equation (14) is also dimensionless as written. Formulation of the particular solution problem using section equations of motion in this form will yield dimensionless particular solutions in terms of the dimensionless axial location and time.

There are some advantages to formulating a telescoping beam system eigenproblem or unforced response problem in dimensionless form. Presentation of nondimensionalized eigensolution permits a limited number of analyses to generate data that represents the solution to an infinite number of physical problems. Such an approach to data display is analogous to that often used with solutions for stress concentration factors and hydrodynamic journal bearings.

There are also disadvantages to this approach. Numerical values for the dimensionless natural frequencies have no physical meaning, making it difficult to interpret the results in the context of an actual system.

### 2.3 Display of Dimensionless Solution Results

When calculated for a specific geometric case, the dimensionless natural frequencies of equation (11) represent the natural frequencies for any telescoping beam with the same number of segments, identical boundary conditions, and the same  $\alpha^{[i]}$  values on a segment-by-segment basis. The dimensionless natural frequencies then can be displayed as a function of dimensionless geometric parameters such as normalized net length or dimensionless overlap ratio. This approach is used in the following analysis and representative charts (Section 3). To recover the actual natural frequencies requires only that the dimensionless values be multiplied by the reciprocal of the reference constant in equation (12) such as

$$\omega_n = \bar{\omega}_n \sqrt{\frac{E_r I_r}{\rho_r A_r L_r^4}} \quad (17)$$

where  $n$  is the modal index.

Parametric display of the normal modes is a special issue. Unlike the natural frequency, a normal mode may not appear to change much even though physical parameters are varied dramatically. It is difficult to characterize a “shape” by a number. The modes are intrinsically normalized, so additional operations on the displacement data set do nothing to further generalize the results. However, the axial location,  $x$ , should be normalized for consistency.

One display option for nondimensionalized modes is to display a plot of a normal mode of interest (the first mode, for example) for a baseline configuration and additional plots for parametric variations upon the baseline configuration. This approach will certainly give a qualitative sense of how design variations might affect the mode shape, but it cannot represent the modes for a wide family of solutions.

Another display approach is to characterize a continuous system normal mode not by the displacement pattern itself, but instead, by discrete parameters that might be important from a

design perspective. Such parameters might include the axial location of the maximum modal displacement, the axial location of nodal points, and modal displacement at other critical locations. Even this approach has limitations. The location of the maximum modal displacement may be absolutely insensitive to parametric changes of the type most likely to be seen in a telescoping structure. For example, the maximum modal displacement of a telescoping cantilever beam will occur at the free end on all modes, and will tend to remain there as the beam extends or retracts.

The position of nodes or anti-nodes is an excellent way to characterize a nondimensionalized mode shape. Knowledge of the basic geometry of the structure and constraints, coupled with knowledge of the node locations permits an experienced designer to precisely visualize the modal displacement pattern. In addition, nodes and anti-nodes may be an important design parameter. Locating a harmonic excitation source at a nodal point of a mode corresponding to the excitation frequency will limit the motion of the source. Anti-nodes may be ideal locations for passive damping added to control the motion of a problem mode. Nodal points of resonating structures may be ideal connection points for substructures that need to be isolated from vibration.

The primary limitation to parametrically characterizing mode shapes by the location of nodes is that the motion of systems vibrating in the fundamental (lowest) modes is generally in-phase, and the normal mode will have no nodes. This is true of a cantilevered telescoping beam that is the subject of the present study. Unfortunately, the first mode is often a critical mode for a system. Broadband, impact-like inputs tend to excite lower modes more strongly than higher modes, and the damping ratio of the lower modes will be lower than for higher modes. Thus, vibration is more likely to begin for the lowest modes, and then more likely to persist.



### 3. Beam Deployment Mechanisms

The most important operational parameter associated with a telescoping structure is the net length,  $L$ . Regardless of whether the structure is used to position objects (cranes, robotic actuators) or receive electromagnetic signals (antennae), the net length will either be prescribed, or otherwise critical to optimal system performance. For a two-segment structure, fixing the net length fixes the overlap ratio, and hence, the entire beam configuration. However, for beams with three or more segments, the beam configuration can be modified independently of  $L$ , provided that internal segments can be separately controlled. The kinematics of deployment for such systems varies. For a very simple system such as a car antenna, only the end-segment is directly moved. Motion of the middle segments is controlled by a combination of friction and limit stops at the segment ends. End segment actuation often yields sequential deployment (relative motion of only one segment at a time), which in turn will result in unequal lengths for the overlap sections. For a system carrying nominal loads, sequential deployment is not a problem.

For heavily loaded structures like cranes, an effort may be made to create proportional deployment. Here the moving segments deploy simultaneously to maintain a constant ratio among the overlap section lengths, which will tend to maximize strength. This type of deployment requires that each segment have its own actuating mechanism. The actuating mechanism may consist of a friction wheel or rack and pinion (Figure 3.1a), a cable, band, belt or chain drive (Figure 3.1b), leadscrews (Figure 3.2c), or other devices.

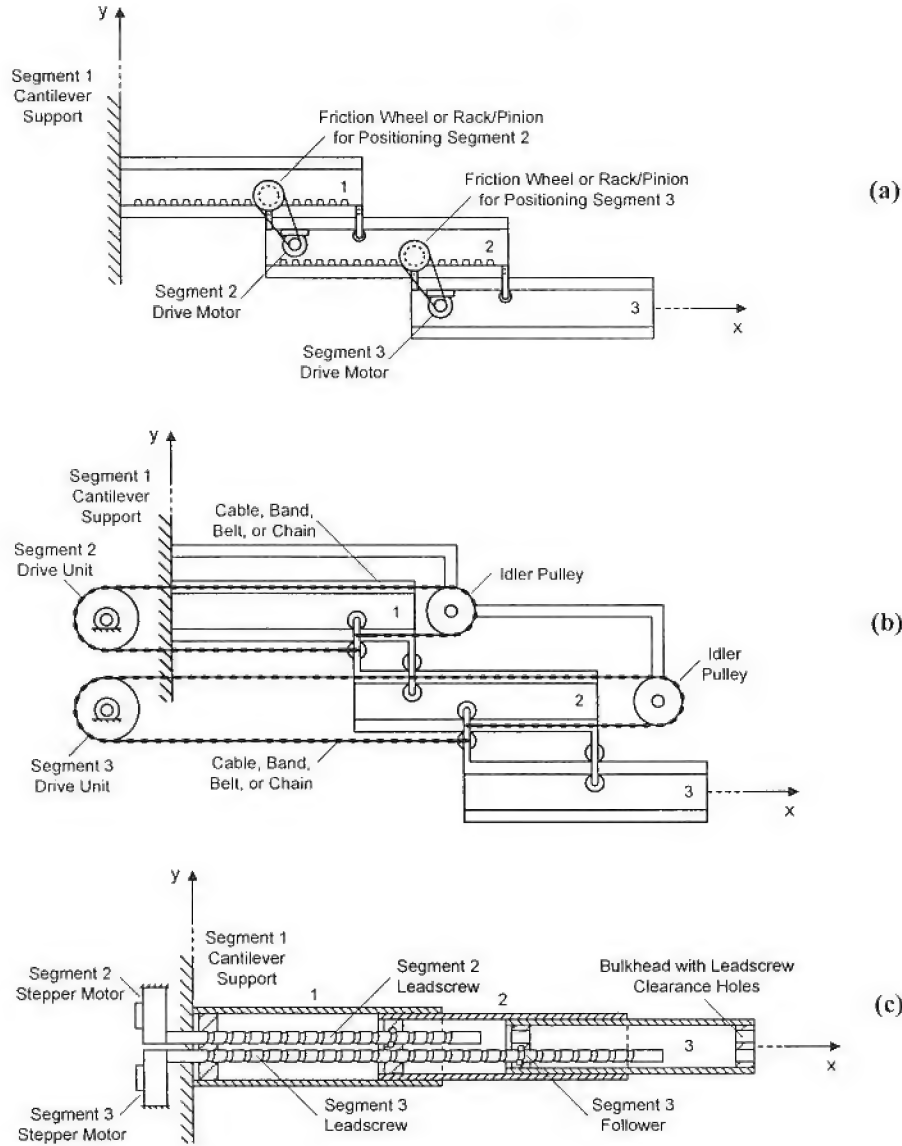


**Figure 3.1. Three-segment telescoping cantilever beam configurations suitable for center-section configuration control. (a) Overlapped beam with segment 2 and segment 3 positioned relative to their supporting sections using a friction wheel or rack and pinion. (b) Overlapped beam with segment 2 and segment 3 positioned globally using a cable, band, belt, or chain drive. (c) Concentric beam with segment 2 and segment 3 positioned globally using leadscrews.**

### 3.1 Response Control Using Internal Segment Positioning

Figure 3.2 illustrates how the configuration of beams with three or more segments may be modified independently of  $L$ , provided that the moving segments can be separately controlled. In addition to maximizing strength or stiffness, middle segment positioning can be used to control the dynamic characteristics of the beam. For example, it should be possible to:

- Change a natural frequency that is being excited by a problematic input harmonic without altering a required deployment length,  $L$ .
- Maintain a prescribed natural frequency despite changes in  $L$ . Such an ability might be useful for systems “tuned” for a particular function, such as vibrating conveyors.
- Minimize end deflections when the beam is subject to axially-moving transverse loads.

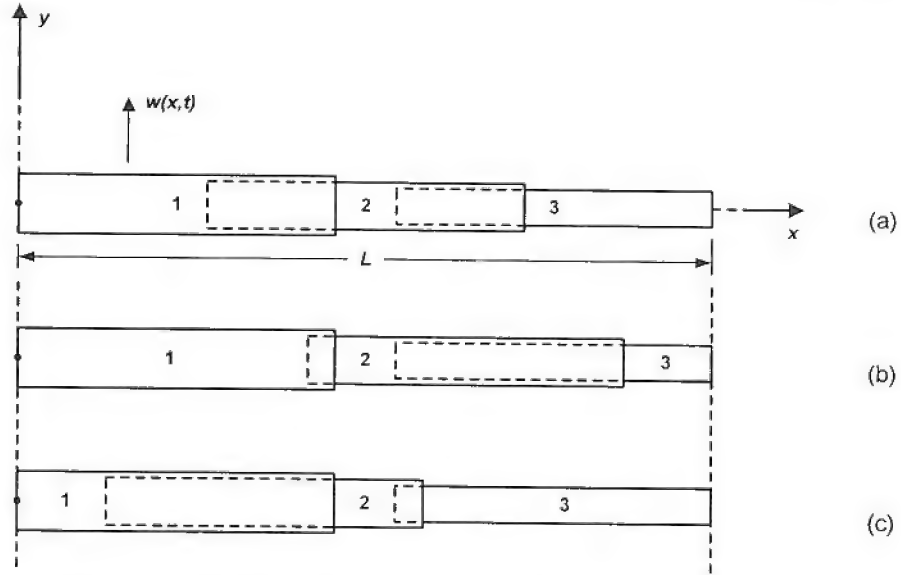


Figure 3.2. Three-segment/five section telescoping beam with independently controllable middle segment. (a) Beam configuration with center section at a “neutral” location chosen to equalize the length of the overlapped segments. (b) Beam configuration with center section moved forward toward the free end. (c) Beam configuration with center section moved aft toward the fixed end (characteristic of sequential deployment).

### 3.2 Example Case of a Three-Segment Telescoping Beam

Without loss of generality, consider an overlapped beam with three independent segments and five sections. Assume that the segment properties are chosen to yield identical values for segment length,  $L_s$ , modulus of elasticity,  $E$ , segment area moment of inertia,  $I_s$ , segment area,  $A_s$ , and segment density,  $\rho$ . Furthermore, assume that the overlapped sections have interface conditions yielding an arithmetically increased moment of inertia:

$$I_{\text{overlapped}} = n^3 I_s \quad (18)$$



Here  $n$  is the number of segments making up the overlapped section ( $n = 2$  or  $n = 3$ , depending upon the level of deployment). The beam will have up to five sections, as illustrated in Figure 3.2. Also, assume that the overlap between adjoining segments can go to zero (rare in physical systems due to the need for the segments to provide bulkheads, stops, and mutual supports, and that adjoining segments can be fully overlapped (quite common with physical systems). To further generalize the results, use the dimensionless form of the equation of motion with the overlap among the segments characterized by the overlap ratio,  $a/b$  (Figure 3.3).

First consider the case of proportional deployment and retraction. Here  $a/b = 1.0$  for both processes. The dimensionless length,  $L/L_1$ , will vary between 1.0 and 3.0. For a given  $L/L_1$  value, the system will have the same physical configuration, modal parameters, and response characteristics during deployment and retraction. Interestingly enough, proportional deployment/retraction does not maximize static stiffness. Because of the internal bending moment distribution (zero at the free end, maximized at the fixed end), configurations with somewhat more overlap between segments 1 and 2 will tend to be more stiff.

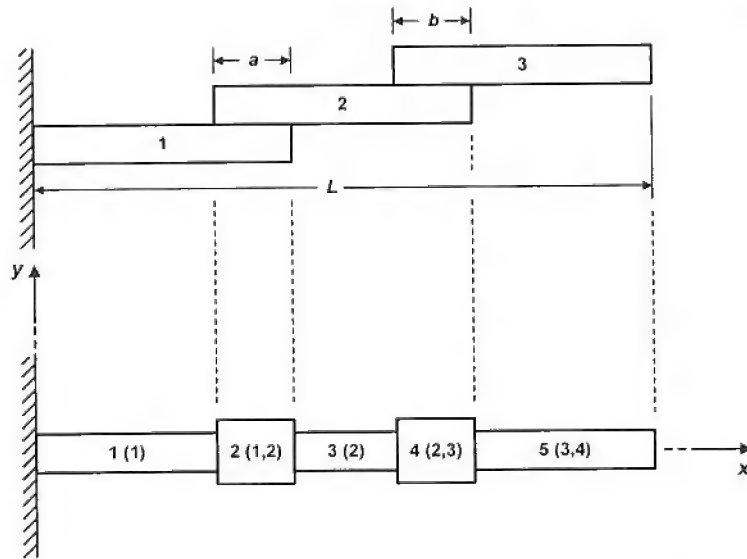


Figure 3.3. Segment configuration and section diagram for a three-segment/five section telescoping beam with independently controllable middle segment. On the section diagram, the first number identifies the section, while the numbers in parenthesis indicate the segment or segments forming the section. The configuration depicted is a “typical” configuration, with no triple-overlap.

Sequential deployment or retraction may be implemented intentionally with a control system, or may occur due to differences in the friction forces in the overlap sections. The motion of segment 2 relative to segment 1 and segment 3 will depend upon the relative magnitude of the friction force between the segment 1/segment 2 overlap section and the segment 2/segment 3 overlap section (sections 2 and 4, respectively in Figure 3.3). These friction forces will come from two different sources: physical supports at the overlap section ends, and relative motion between the segment portions making up the overlap sections. The first source will tend to remain constant as the length of the overlap sections,  $a$  and  $b$ , change. The second source may be expected to change during deployment. Larger values for  $a$  or  $b$  will result in correspondingly larger friction forces.

Consider a case where the axial friction forces are constant, with the friction force within section 2 greater than that within section 4 ( $F_{fa} > F_{fb}$ ). Under these circumstances, segment 3 will move first during deployment, with  $a/L_1$  remaining 1.0, and  $b/L_1$  varying between 1.0 and 0.0. Similarly,  $a/b$  varies from 1.0 at  $L/L_1 = 1.0$  (start of deployment), to  $\infty$  at  $L/L_1 = 2.0$ . At this point, segment 3 is fully extended relative to segment 2. Segment 3 now pulls segment 2 and both begin to move as a rigid body relative to segment 1. The overlap ratio remains at  $a/b = \infty$  until the beam is fully extended at  $L/L_1 = 3.0$ .

Sequential retraction under these friction conditions follows a different process. Segments 1 and 2 initially remain fixed ( $a/L_1 = 0.0$ ) while segment 3 moves from a position with  $b/L_1 = 0.0$  to another with  $b/L_1 = 1.0$  ( $a/b = 0.0$ ). Segment 2 and 3 then begin to retract together, and  $a/L_1$  increases from 0.0 to 1.0 ( $a/b$  increases from 0.0 to 1.0). It is critical to note that under these friction conditions, and for a given  $L/L_1$  value, sequential deployment/retraction systems will have different physical configurations during deployment and retraction, and the modal parameters and physical response will also differ.

### 3.2.1 Results for the Fundamental Mode

For a three-segment system it is possible to view a comprehensive set of specific modal response parameters by plotting the parameter as a function of  $L/L_1$  for different  $a/b$  ratios.

Consider the nondimensionalized fundamental natural frequency,  $\bar{\omega}_1 = \omega_1 \sqrt{\rho_1 A_1 L_1^4 / (E_1 I_1)}$ . Figure 3.4 shows these values for the full range of physically possible  $L/L_1$  values ( $1.0 \leq L/L_1 \leq 3.0$ ) and  $a/b$  values ( $0.0 \leq a/b \leq \infty$ ). When viewing this figure, one is struck by its similarity to the charts used depict families of solutions for hydroscopic journal bearings and form stress concentration factors. Like these familiar plots, the dimensionless fundamental frequency plot represents a comprehensive collection of solutions, and can be used as a design tool.

Consider first the proportional deployment case of  $a/b = 1.0$ . The fundamental frequency begins at a maximum value of  $\bar{\omega}_1 = 10.55$  at  $\bar{L} = L/L_1 = 1.0$ , and decreases in a nonlinear fashion<sup>2</sup> to  $\bar{\omega}_1 = 0.391$  at  $\bar{L} = L/L_1 = 3.0$ . Increasing the  $a/b$  ratio increases  $\bar{\omega}_1$  for a given length. This trend is explained by the fact that higher  $a/b$  ratios correspond to segment 2 closer to the fixed support, which will tend to reduce the effective mass and increase the effective stiffness. Either effect will tend to increase the system natural frequencies. Note that the  $a/b > 1.0$  curves begin at  $L/L_1$  values greater than 1.0 due to physical configuration constraints. This starting value corresponds to the case of maximized  $b$  values, yielding

$$\left( \frac{L}{L_1} \right)_{initial} = 2 - \frac{1}{a/b}, \quad a/b \geq 1.0 \quad (19)$$

---

<sup>2</sup> Figure 3.4 is presented as a semilog plot to emphasize the dispersion among the different  $a/b$  curves. When plotted on linear scales, the curves retain the same general shape (compare Figure 7.4 with Figure 7.6).



Reducing the  $a/b$  ratio below 1.0 reduces the effective stiffness, increases the effective mass, and thus decreases  $\bar{\omega}_1$ . Again, these curves all have starting values greater than 1.0 due to physical constraints, with the initial values given by:

$$\left(\frac{L}{L_1}\right)_{initial} = 2 - a/b, \quad a/b \leq 1.0 \quad (20)$$

Figure 3.5 is a rescaling of the fundamental natural frequency solution data to enhance the region where the  $a/b$  curves converge at  $L/L_1 = 3.0$ . Note that the curves do not cross; thus, all solutions for the fundamental frequency are unique. It is possible to interpolate between curves to estimate intermediate solution values.

Figure 3.6 shows the possible solution envelope for the fundamental natural frequency of this three-segment beam. The plot is based upon the data displayed in Figure 3.4, with the exception that it is plotted on linear scales. Four points of interest are numbered. Point 1 represents the beam in its fully retracted position. This configuration corresponds to the minimum possible beam length, with  $a/b = 1.0$ . Point 2 corresponds to a half deployed beam, with segment 2 not having moved (segment 3 alone has deployed), and  $a/b = \infty$ . Point 4 also corresponds to a half deployed beam, but with  $a/b = 0$  (for example, segments 2 and 3 may have deployed simultaneously from a fully retracted configuration). Finally, point 3 represents the fully deployed beam, with  $L/L_1 = 3.0$ . All  $a/b$  curves converge to this point as the beam reaches its maximum length.

Together, any set of beam configurations leading from point 1 to point 3 constitutes a deployment process. Any set of beam configurations leading from point 3 to point 1 constitutes a retraction process. The proportional deployment and retraction process (constant  $a/b$  value of 1.0) have already been described. The configurations at the boundaries of the configuration envelope correspond to special processes. For example, configurations 1-2 and 2-3 represent a

sequential deployment process for the constant friction case of  $F_{f,a} > F_{f,b}$ . Segment 3 opens fully while segments 1 and 2 are stationary (increasing  $a/b$  ratio until  $L/L_1 = 2.0$ ), and then pulls segment 2 open ( $a/b = \infty$ ). For the same friction conditions, the retraction process follows the bottom of the envelope, 3-4, and 4-1. The retraction process begins with segment 3 moving, while segment 2 remains stationary ( $a/b = 0$ , point 3 to point 4). At point 4, segment 3 is fully retracted relative to segment 2 and begins pushing segment 2 closed (increasing  $a/b$  ratio, point 4 to point 1) until the entire beam is retracted ( $a/b = 1.0$ ). Thus, sequential deployment and retraction follow distinctly different processes as defined by the segment configurations, and for a given net length, the beam will exhibit different modal parameters and response characteristics depending upon whether it is being deployed or retracted.

If the friction force between segments 2 and 3 remains greater than that between segments 1 and 2 ( $F_{f,b} > F_{f,a}$ ), sequential deployment will proceed from points 1-4 in Figure 3.6 (segments 2 and 3 moving together until segment is fully extended), and then from points 4-3 (segment 3 moving alone). Retraction will follow a process from 3-2 and 2-1. Again, the configuration sequence will be different, resulting in differences in the response and modal parameters.

Regardless of the axial friction force conditions, it is unlikely that an end-deployed beam will follow identical deployment and retraction processes without some sort of external control. However, if segment 2 and segment 3 can be moved independently, any desired deployment or retraction process within the envelope may be prescribed.

Inspection of the configuration envelope of Figure 3.6 shows that for a given value of the fundamental frequency, the beam can be configured to maintain that natural frequency for a range of net lengths. For example, the beam can maintain  $\bar{\omega}_1 = 5.0$  for  $L/L_1$  values between approximately 1.05 and 1.30. To do so requires that the center segment be moved as far toward the fixed support as possible for the higher  $L/L_1$  value, and as far toward the free end as possible

for the lower  $L/L_1$  value. Again, such control requires independent positioning mechanisms for segments 2 and 3, along with system elements that measure two lengths (linear potentiometers or LVDTs, for example) and adjust the center segment position to an appropriate value (perhaps obtained from a lookup table). Figure 3.7 depicts the dimensionless length variation  $(L_{\max}/L_1 - L_{\min}/L_1)$  over the range of possible fundamental frequency values. This variation increases gradually from zero at the fully retracted configuration (point 1 on Figure 3.7), to a maximum value of  $L_{\max}/L_1 - L_{\min}/L_1 = 0.81$  when  $L_{\max}$  is near the half-retracted/extended position (point 2 on Figure 7.7). It then rapidly decreases due to the shape of the configuration envelope to a value of zero at the fully extended location (point 3 on Figure 3.7).

The configuration envelope also implies that it is possible to vary the first natural frequency while holding the beam net length constant. Again, this effect is achieved by moving segment 2 independently of segment 3. Figure 3.8 shows the possible nondimensionalized fundamental natural frequency range as a function of  $L/L_1$ . From the fully retracted position (point 1 on Figure 3.8),  $\bar{\omega}_{1,\max} - \bar{\omega}_{1,\min}$  increases very rapidly from zero to a maximum value of 4.75 at  $L/L_1 = 1.05$ . It then decreases back to a value of zero (point 3 on Figure 3.8). The point identified as “(2,4)” on Figure 3.8 corresponds to an inflection point at  $L/L_1 = 2.0$ . This point in turn corresponds to the configurations marking the transition from a fixed  $a/b$  ratio to a variable  $a/b$  ratio (points 2 and 4 on Figure 3.6).

The peak marking the maximum  $\bar{\omega}_{1,\max} - \bar{\omega}_{1,\min}$  value is so prominent and so much like a singularity in appearance that it seems to be the result of configuration-related effect. However, no type of configuration change corresponds to the  $L/L_1$  value of 1.05 at the peak. This result may be seen by normalizing the dimensionless natural frequency range by dividing by  $\bar{\omega}_{1,\max}$ . The resulting plot of  $(\bar{\omega}_{1,\max} - \bar{\omega}_{1,\min})/\bar{\omega}_{1,\max}$  is shown in Figure 3.9. The singularity-like nature of



the peak is seen to be nothing more than the result of a very rapid increase in the dimensionless natural frequency range. This rapid increase is moderated by dividing by  $\bar{\omega}_{l,\max}$ , which is rapidly increasing but continuous in this  $L/L_1$  neighborhood. The new plot is also continuous here. Figure 3.9 also shows that the normalized natural frequency range remains greater than 50 percent of the maximum natural frequency for a significant portion of the retraction range ( $1.05 \leq L/L_1 \leq 2.15$ ), and reaches a maximum value of 71.3 percent.

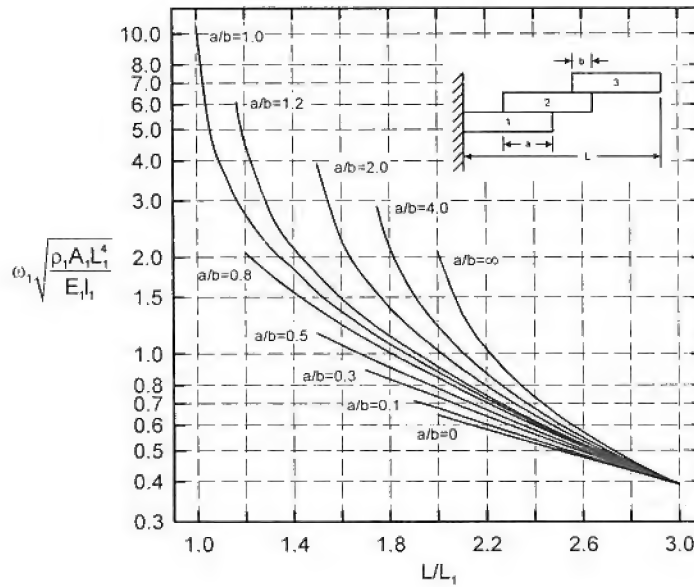


Figure 3.4. Nondimensionalized fundamental natural frequency values as a function of nondimensionalized net length and section overlap ratio for a three segment telescoping beam with fixed/free end conditions, uniform segment properties, identical segment lengths, and moments of inertia for individual segments given by  $I = n^3 I_1$ , where  $n$  is the number of segment in the overlapped region (equivalent to solid rectangular cross sections with no interface slippage). All parameters, including lengths, are normalized with respect to the values of the first section.

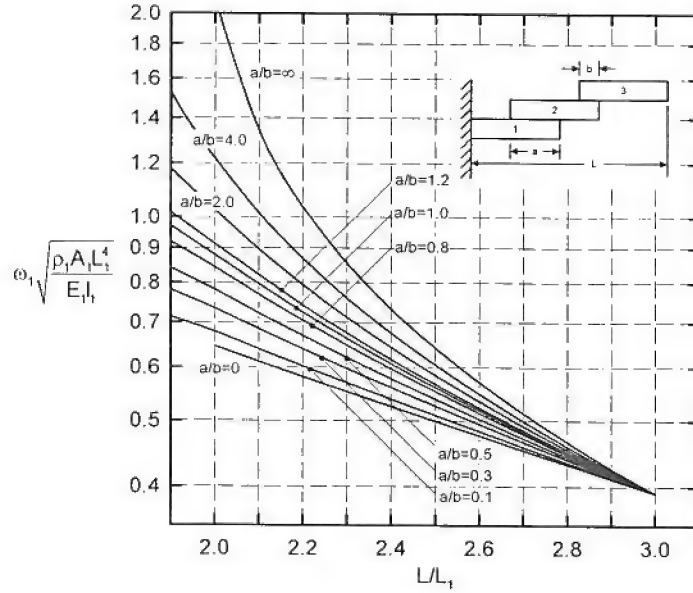


Figure 3.5. Data from Figure 3.4 in the region without triple overlap ( $2.0 \leq L/L_1 \leq 3.0$ ).

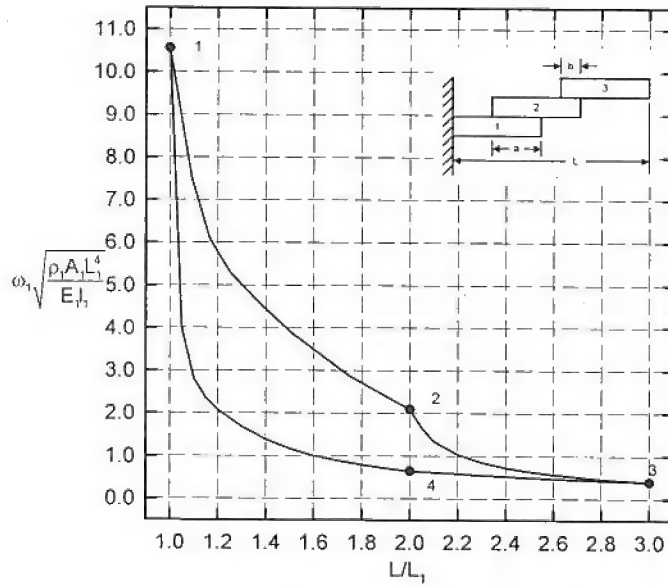


Figure 3.6. Possible solution envelope for the nondimensionalized fundamental natural frequency values as a function of net beam length and section overlap ratio. Three section telescoping beam with fixed/free end conditions, uniform segment properties, identical segment lengths, and moments of inertia for individual segments given by  $I = n^3 I_1$ , where  $n$  is the number of segments in the overlapped region (equivalent to solid rectangular cross sections with no interface slippage). All parameters, including lengths, are normalized with respect to the values of the first segment.

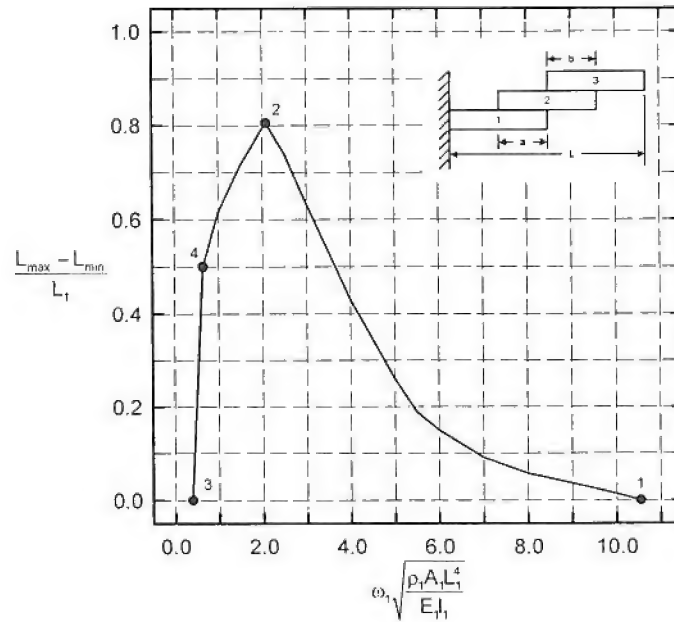


Figure 3.7. Dimensionless length variation possible at constant values of nondimensionalized fundamental natural frequency. Three segment telescoping beam with fixed/free end conditions, uniform segment properties, identical segment lengths, and moments of inertia for individual segments given by  $I = n^3 I_1$ , where  $n$  is the number of segments in the overlapped region (equivalent to solid rectangular cross sections with no interface slippage). All parameters, including lengths, are normalized with respect to the values of the first segment.

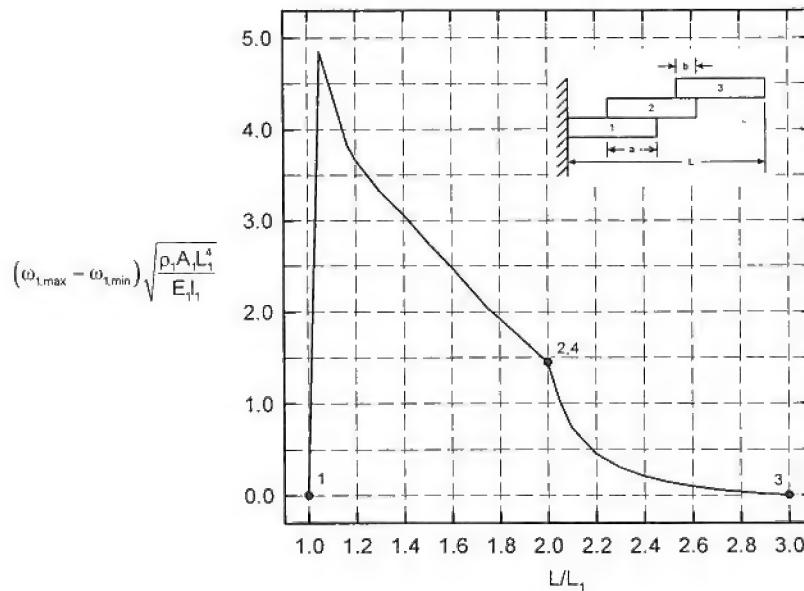


Figure 3.8. Nondimensionalized fundamental natural frequency range possible at constant dimensionless length values. Three segment telescoping beam with fixed/free end conditions, uniform segment properties, identical segment lengths, and moments of inertia for individual segments given by  $I = n^3 I_1$ , where  $n$  is the number of segments in the overlapped region (equivalent to solid rectangular cross sections with no interface slippage). All parameters, including lengths, are normalized with respect to the values of the first segment.

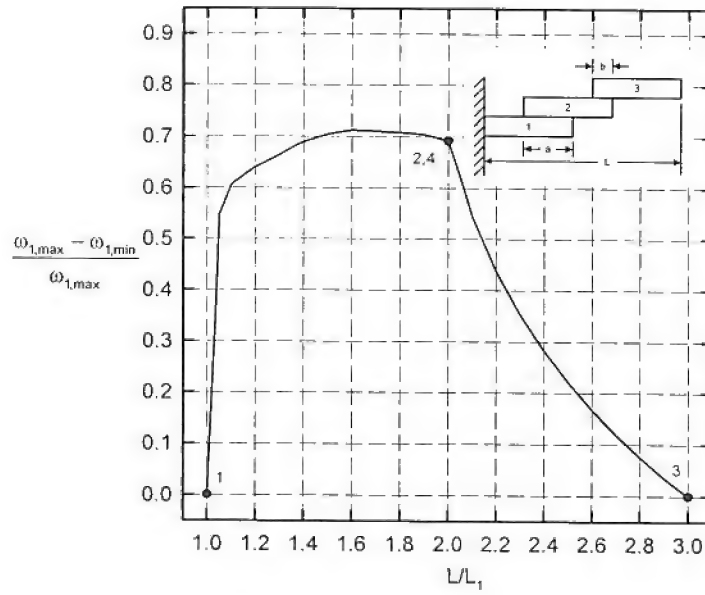


Figure 3.9. Nondimensionalized fundamental natural frequency range data from Figure 3.8 normalized by the maximum natural frequency possible at the  $L/L_1$  value.

### 3.2.2 Results for the Second Mode

Now consider the variation of the nondimensionalized second natural frequency with beam configuration. Figures 3.10-3.15 are the second mode analogs to Figures 3.4-3.9 for the first mode. Figures 3.10 and 3.11 depict the natural frequency values for different  $a/b$  ratios as a function of  $L/L_1$ . Figure 3.12 is the mode 2 configuration envelope. One characteristic of these curves is immediately apparent. In contrast to the well-ordered, evenly dispersed  $a/b$  curves seen in Figures 3.4 and 3.5, the  $a/b$  curves for the second mode seem more chaotic. Rather than being in the middle of the mode 2 configuration envelope, the proportional deployment curve ( $a/b = 1.0$ ) lies near the top of the envelope. Any deviation from proportional deployment tends to reduce  $\bar{\omega}_2$  at a given  $L/L_1$  value. More importantly, the curves intersect at various points. As an example, consider the  $a/b = 0.0$  and  $a/b = \infty$  curves in Figure 3.11. At a net length ratio of  $L/L_1 = 2.08$ , the curves intersect. Thus, for this net length, the beam has the same second natural frequency in the two extreme positions of the center segment (fully forward for  $a/b = 0.0$  and



fully aft for  $a/b = \infty$ ). For a wide range of lengths ( $1.3 \leq L/L_1 \leq 3.0$ ), the  $a/b = 1.0$  and  $a/b = 1.2$  configurations have very close natural frequency at a given length.

The mode 1 configuration envelope was comprised entirely of configurations where the center section was as close to the fixed end of the beam as possible (process 1-2-3 in Figure 3.6), or as close to the free end as possible (process 1-4-3 in Figure 3.6). For the second mode, these extreme configurations no longer lie on the edge of the configuration envelope. Sequential deployment/retraction process will tend to lie within the envelope.

It is clear that middle segment manipulation has decreasing effect upon the higher modes.<sup>3</sup> As a result, the degree of possible natural frequency control is greatest for mode 1, and significantly reduced for mode 2. For the first mode, the maximum length variation for a given natural frequency was  $L_{\max}/L_1 - L_{\min}/L_1 = 0.81$ . For mode 2 the corresponding value is only 0.30 (Figure 3.13). The normalized natural frequency range,  $(\omega_{1,\max} - \omega_{1,\min})/\omega_{1,\max}$ , was 0.712 for mode 1 and 0.392 for mode 2 (Figure 3.15).

A physical explanation for the reduced effect of center segment manipulation on the higher modes is the presence of nodal points in the higher eigenfunctions. Physical changes near a nodal point (for example application of an external passive element such as a damper or spring) will have little effect upon the corresponding modal response (the change will, however, affect, the other modes). Furthermore, during a deployment or retraction process, the effect of a center changes will tend to fluctuate while as the overlap sections pass through the nominal node. This variation explains the fluctuations seen in the deployment/retraction process curves in Figures 3.10 and 3.11 to occur near the nodes associated with the second eigenfunction.

---

<sup>3</sup> It is important to note here that while center segment manipulation has a smaller effect on the mode 2 characteristics, a complete deployment or retraction process results in a greater change in the second nondimensionalized natural frequency (a range between 0.391 and 10.548 for mode 1, and a range between 2.448 and 66.104 for mode 2).

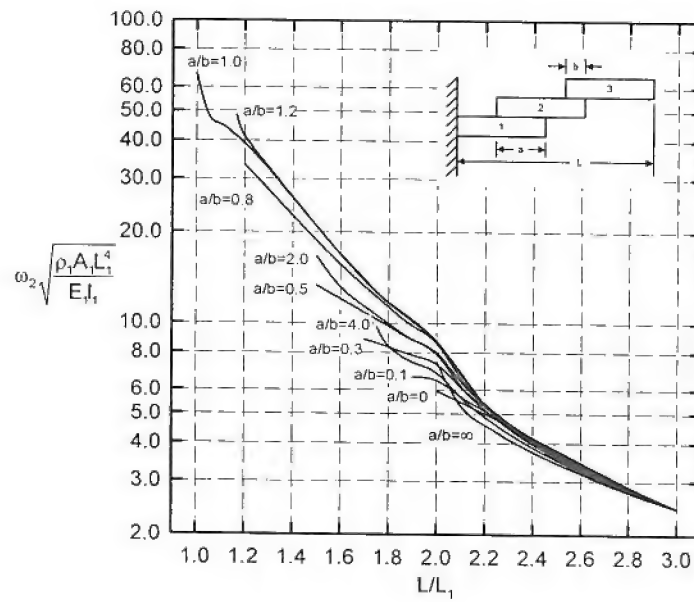


Figure 3.10. Nondimensionalized second natural frequency values as a function of nondimensionalized net length and segment overlap ratio for a three segment telescoping beam with fixed/free end conditions, uniform segment properties, identical segment lengths, and moments of inertia for individual segments given by  $I = n^3 I_1$ , where  $n$  is the number of segments in the overlapped region (equivalent to solid rectangular cross sections with no interface slippage). All parameters, including lengths, are normalized with respect to the values of the first segment.

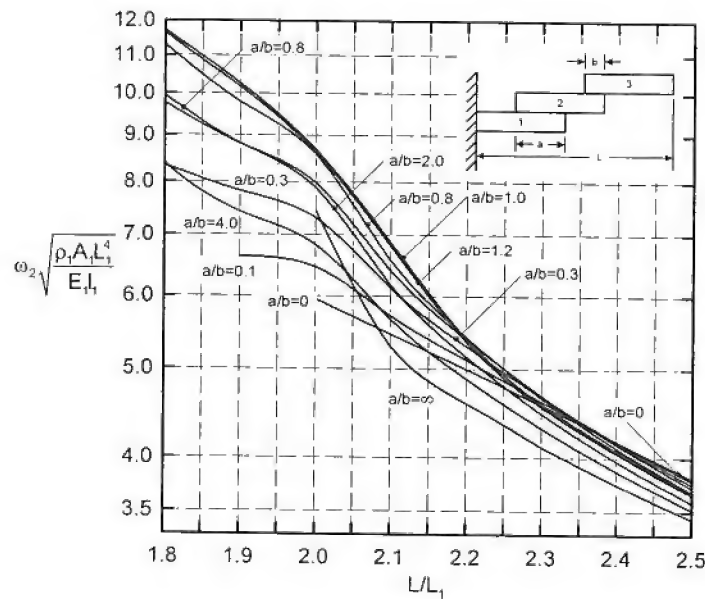


Figure 3.11. Data from Figure 3.10 in a portion of the region near the nominal nodal point for the fully extended configuration ( $x = 2.3504$ ).

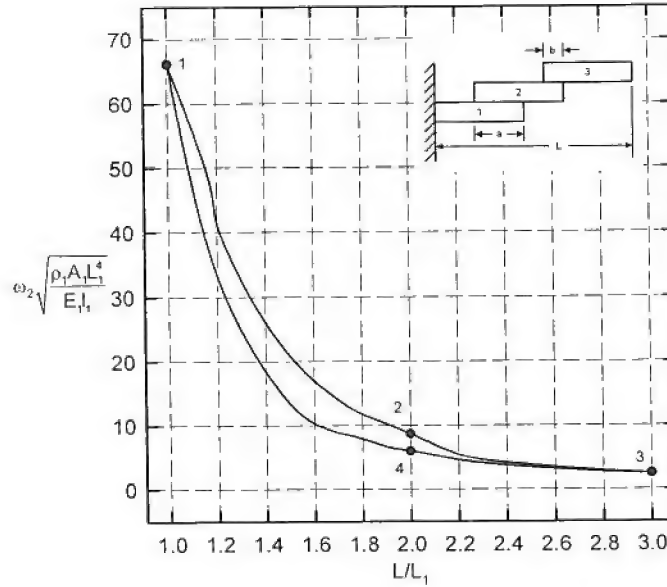


Figure 3.12. Possible solution envelope for the nondimensionalized second natural frequency values as a function of net length and segment overlap ratio. Three segment telescoping beam with fixed/free end conditions, uniform segment properties, identical segment lengths, and moments of inertia for individual segments given by  $I = n^3 I_1$ , where  $n$  is the number of segments in the overlapped region (equivalent to solid rectangular cross sections with no interface slippage). All parameters, including lengths, are normalized with respect to the values of the first segment.

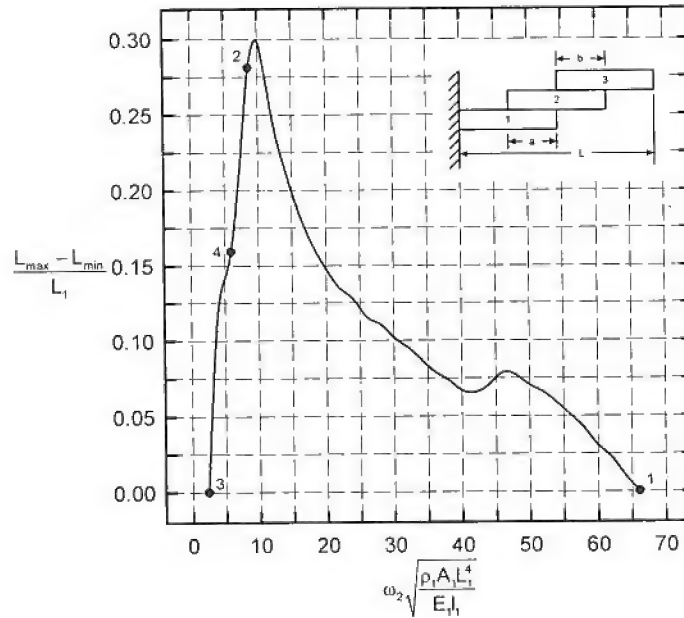


Figure 3.13. Dimensionless length variation possible at constant values of nondimensionalized second natural frequency. Three segment telescoping beam with fixed/free end conditions, uniform segment properties, identical segment lengths, and moments of inertia for individual segments given by  $I = n^3 I_1$ , where  $n$  is the number of segments in the overlapped region (equivalent to solid rectangular cross sections with no interface slippage). All parameters, including lengths, are normalized with respect to the values of the first segment.

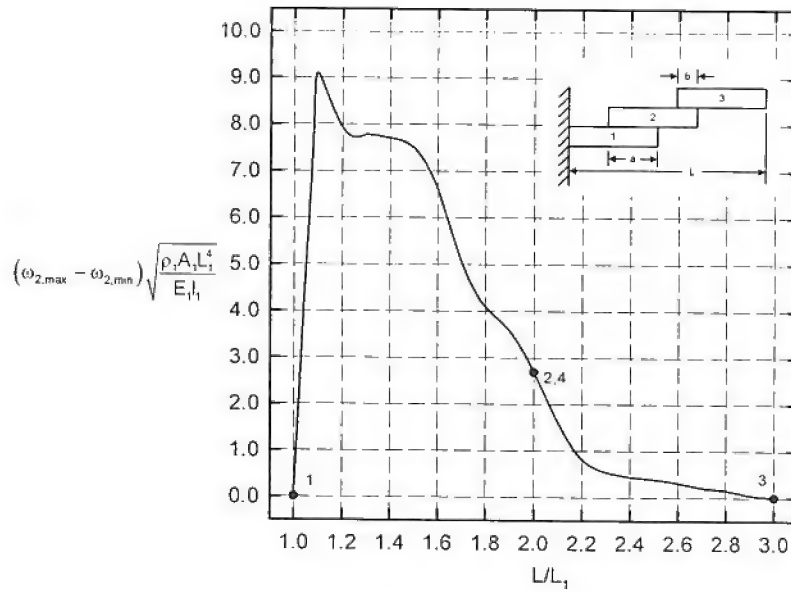


Figure 3.14. Nondimensionalized second natural frequency range possible at constant dimensionless length values. Three segment telescoping beam with fixed/free end conditions, uniform segment properties, identical segment lengths, and moments of inertia for individual segments given by  $I = n^3 I_1$ , where  $n$  is the number of segments in the overlapped region (equivalent to solid rectangular cross sections with no interface slippage). All parameters, including lengths, are normalized with respect to the values of the first segment.

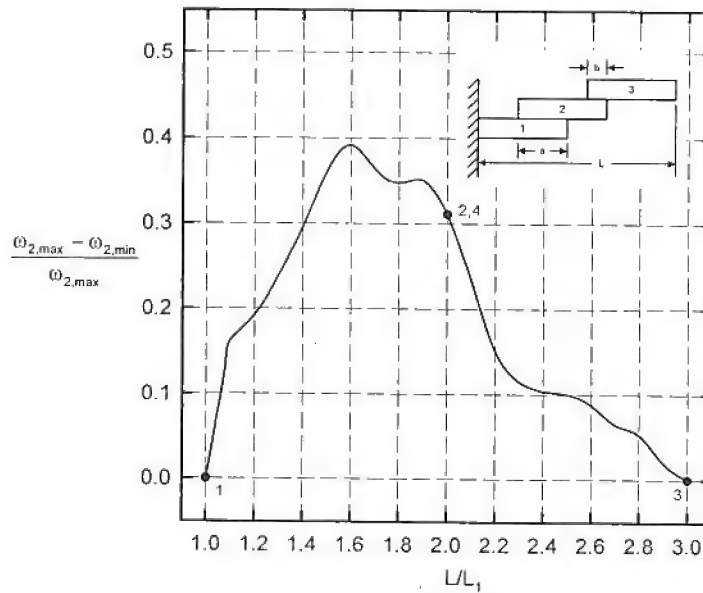


Figure 3.15. Nondimensionalized second natural frequency range data from Figure 3.14 normalized by the maximum natural frequency possible at the  $L/L_1$  value.

#### 4. CONCLUSION

Investigation of the kinematic behavior and configuration control of telescoping beam with three or more segments in Section 3 show that the response of these beams can be modified independently of the total length by using the internal segment(s) as a controlling tool (section 3.1). Two classifications for deployment/retraction mechanisms are proposed: proportional and sequential. The different mechanisms' effect on the system's physical configuration, modal parameters, and response characteristics during the control process is considered in section 3.2. No comparable investigations or analyses the extension and retraction motion of segmented structures is found in the open literature, nor has the central role of friction been previously described.

A primary purpose of the research presented in Section 3 was to generalize the telescoping beam modal results to facilitate their use by designers. To achieve this goal, the segmented beam equation of motion was presented in dimensionless form, which in turn allowed determination of natural frequencies nondimensionalized with respect to the physical and geometric properties of the first segment:

$$\bar{\omega}_n = \omega_n \sqrt{\frac{\rho_1 A_1 L_1^4}{E_1 I_1}} \quad (21)$$

The nondimensionalized natural frequency plots of Figures 3.4-3.5 and 3.10-3.11 can be a fundamental contribution to the body of knowledge on configurable vibration systems. These plots are similar in concept and application to the very well known charts used to capture solution data for stress concentration factors and hydrodynamic journal bearing parameters. In this research the nondimensionalized plots were obtained only for the fundamental and second natural frequencies; however the approach can easily be extended to higher modes. Using these



techniques and plots as a design tool can substantially reduce the amount of time and effort expended in calculating natural frequencies for multi-segment cantilever beam structures.

Cantilever boundary conditions - one fixed and one free end - are by far the most typical constraints found with telescoping beams, and accordingly, this research has focused on this case. However, a few other configurations may be found in practice. While by no means exhaustive, Figure 8.1 shows three representative examples. The beam of Figure 8.1a has a first segment with its ends constrained by simple supports. The two-segment design depicted is a reasonable model for some actuators. Figure 8.1b shows another practical configuration. For long, horizontal actuators, a cantilever design may be impractical due to excessive free-end sag. The depicted configuration uses a “rolling” simple support at the extreme end. In the case of extremely long telescoping beams of this type, it may be necessary to support all of the moving segments (Fig. 8.1c).

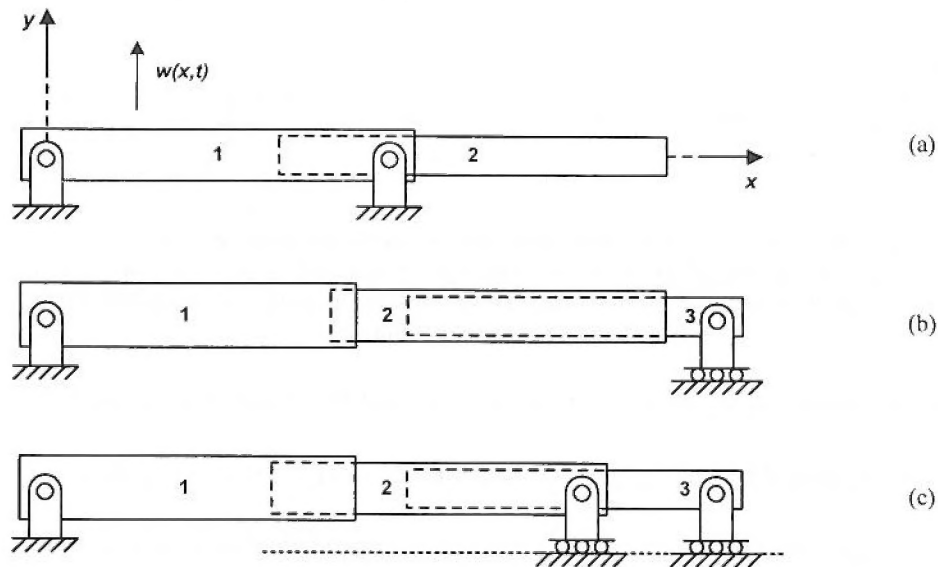


**Figure 8.1. Non-cantilevered telescoping beams with supports that may still be analyzed using the modeling/solution methodologies developed during this research. (a) Actuator with pinned first section, (b) telescoping beam with one fixed simple support and one axially unconstrained simple support on the end segment, (c) telescoping beam with one fixed simple support and axially unconstrained simple supports on each of the moving segments.**

In addition to telescoping beams with atypical constraint conditions, modeling and solution methodologies from this work may be applied to slender structures loaded in bending that cannot be classified as telescoping beams. Figure 8.2a shows a long, continuous primary member with a smaller, secondary sleeve-beam that moves along the primary beam. This model is a good approximation of some overhead cranes. The secondary beam will change the local inertia and compliance characteristics as it moves along the primary. Figure 8.2b depicts a single beam with a single segment that can be transitioned from an open-section configuration to a closed-section configuration by moving a coupler along an open seam. As the coupler closes the seam, it increases the local compliance.

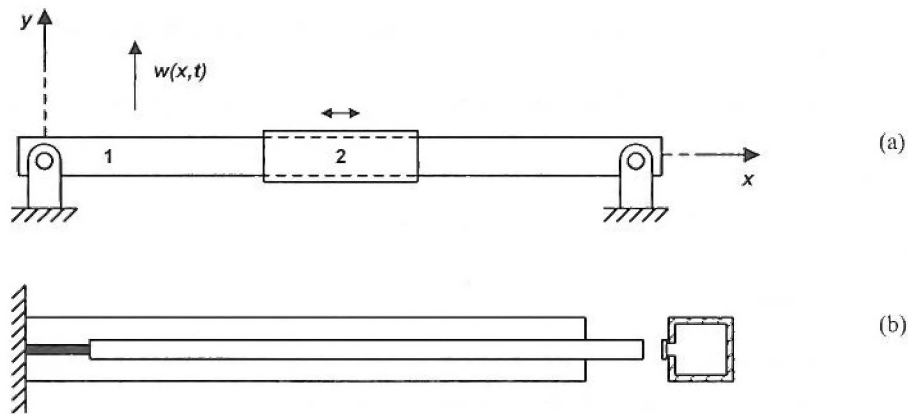


**Figure 8.2. Telescoping beam-like systems suitable for analysis with the modeling/solution methodology developed during this research. (a) Simply supported continuous beam with axially translating center section, (b) single section beam with open/closed section seam control.**

There are no known systems of this type in service, and the detail design needed to implement the concept would be challenging, to say the least. However, the ability to change compliance without significantly modifying the system mass distribution could be very useful for some applications.

## References:

- [1] **Andrusiv, L.P.**, Prater, G., and Richards, C.M., “Dynamic Behavior of Segmented Telescoping Structures in Automotive Systems,” *SAE International Journal of Passenger Cars – Mechanical Systems*, Vol. **1**(1): 238-249, 2009.
  
- [2] **Andrusiv, L.P.** and Richards, C.M., Modeling and Vibration Response of Segmented Flexible Structures, *The VII International Research Conference on Mathematical Problems of Mechanics of Non-Homogeneous Structures*, v.2, pp.156-158, Ukraine, 2006.